Yu.S. Dzyazko [1], V.M. Ogenko [1], Yu.M. Volfkovich [2], V.E. Sosenkin [2], T.V. Maltseva [1], T.V. Yatsenko [1], K.O. Kudelko [1]

COMPOSITE ON THE BASIS OF HYDRATED ZIRCONIUM DIOXIDE AND GRAPHENE OXIDE FOR REMOVAL OF ORGANIC AND INORGANIC COMPONENTS FROM WATER

[1] *Vernadsky Institute of General and Inorganic Chemistry of National Academy of Sciences of Ukraine*
32/34 Academician Palladin Avenue, Kyiv, 03680, Ukraine, E-mail: ogenko@gmail.com
[2] *A.N. Frumkin Institute of Physical Chemistry and Electrochemistry of Russian Academy of Sciences*
31 Leninskii pr., Moscow, 119071, Russia, E-mail: yuvolf40@mail.ru

The aim of the investigation is to develop multifunctional adsorbent, which is able to remove both inorganic ions and molecular organic substances from aqueous solutions. Oxidized graphene has been obtained by Hammer's method. The composite, which includes hydrated zirconium dioxide and graphene oxide (≈ 2 mass. %), has been synthesized by deposition from sol containing dispersed particles of the carbon material. The adsorbent as well as its constituents were investigated with methods of XRD analysis, FTIR spectroscopy, TEM and standard contact porosimetry involving octane (ideally wetting liquids) and water as working liquids. Strong hydration of graphene oxide in water has been found: the volume of micro- and mesopores in water medium is higher than that in octane. It means that the oxidized graphene behaves similarly to ion exchange polymers. This is evidently due to its hydrophilic functional groups (hydroxyle carboxyl and epoxy groups). High specific surface area of graphene oxide reaches 1200 (in the organic solvent) or 2250 $m^2 g^{-1}$ (in aqueous medium). It has been shown that graphene covers the particles of the inorganic matrix loosening its structure within the wide interval of pore size (from 10 nm to 1.5 μm). As found, adsorption isotherms of Pb(II) and $HCrO_4^-$ ions obeys with Langmuir model. The filler improves adsorption of Pb(II) ions increasing the capacity in 1.7 times due to its expressed cation exchange properties. Contrary, anion exchange function of the composite is depressed, since the sheets of graphene oxide screen adsorption centers of the inorganic matrix. Other reason can be electrostatic repulsion of anions due to the shift of the point of zero charge of the composite to acidic field. By reason of the carbon filler, the oxide material acquires the capability to adsorb both slightly dissociated (phenol) and molecular (lactose) organic substances. When the initial content of phenol is 5 mg dm^{-3}, it is possible to reduce its content in water down to maximal permeable concentration. After adsorption, the content of lactose is much lower than this parameter. It means, that the composite provides practically complete removal of organics from water.

***Keywords**: graphene oxide, hydrated zirconium dioxide, standard contact porosimetry, hydrophilic pores, hydrophobic pores, adsorption, lead, chromate, phenol, lactose*

INTRODUCTION

Graphene oxide (GO) is a layered material consisting of nanosheets, a thickness of which is one atom (0.54 nm) [1–4]. As opposed to reduced graphene, vibration spectra for GO indicate carbon-oxygen bonds: C−OH (attributed both to hydroxyl and carboxyl groups), C=O (related to carboxyl groups) and (epoxy groups) [2, 5]. Carboxyl groups are mainly placed along the perimeter of GO scales, hydroxyl and epoxide groups are located on their basal plane [5, 6]. GO is obtained by means of chemical exfoliation of oxidized graphite [7].

Such reagents as $NaNO_3$, $KMnO_4$, H_2SO_4 and H_2O_2 are used. Sometimes the preformed acidic oxidizing medium ($KMnO_4$ and H_2SO_4) is applied to GO synthesis [8].

Similarly to graphene, GO is in a focus of attention, since the materials of this type possess unique physico-chemical properties. Among these properties, high specific surface area (from 560 [9] to 900 $m^2 \ g^{-1}$ [10]) has been reported. These data were measured by the BET method, which involves nitrogen adsorption-desorption. The surface area that is obtained by this manner is lower in comparison with the theoretical value for completely exfoliated and isolated graphene sheets ($\approx 2600 \ m^2 \cdot g^{-1}$ [5]). This disagreement is caused by agglomeration, overlapping and

curling the sheets of graphene. Nitrogen molecules are not capable to penetrate between the graphene sheets under low temperature. As opposed to BET technique, the method of standard contact porosimetry (MSCP) [11, 12], which involves octane as a working liquid, gives the values of 2000–2400 $m^2 \cdot g^{-1}$ [13]. This is possible due to disjoining pressure of octane: this liquid completely wets carbon materials penetrating between graphene sheets. Since the MSCP is confirmed by the IUPAC [14], the obtained magnitudes look rather probable.

Other remarkable properties of GO are excellent mechanical strength [15], dispersibility both in organic solvents [16] and water [17], structural transformability. The last property gives the possibility of adsorption interaction of GO with different materials, such as iron oxide [18], quartz sand [19], kaolin [20, 21], glass [22], composites that include chitosan and oxides of aluminium, zinc or magnesium [23], goethite [24]. The mechanism of adsorption depends on the solution pH. In many cases, electrostatic attraction with the surface of oxide materials and GO scales occurs [23, 24], formation of hydrogen bonds is also considered. Based on the data of IR spectroscopy, complexation of metal ions on goethite surface with –COOH groups of GO is suggested [24]. The interaction between GO and mineral surface gives additional possibilities to develop the composites containing carbon materials.

Highly developed surface of GO, ion exchange groups (carboxyl and hydroxyl) as well as hydrophobic regions allow one to use this material as an adsorbent for removal of toxic mineral and organic components from aqueous solutions: cationic dyes [25–27] (adsorption of anionic dyes is negligible [27]), antibiotics [28], algal toxins [29], deoxyribonucleic acid [30], polycyclic aromatic hydrocarbons [31] and other substances. It should be noted that hydrophylic groups of GO depress adsorption of hydrophobic compounds in comparison with reduced graphene. However, GO is attractive as an adsorbent of toxic inorganic cations: Cd(II) [32–34], Co(II) [32], Cu(II) [33, 34], Zn(II) [33], Pb(II) [33]. Ni(II), U(VI) [34, 35]. Unfortunately, practical application of GO materials in adsorption columns is difficult due to their small particle size, since such particles provide high hydrodynamical resistance. Other important limitation is good dispersibility.

The solution of this problem is to develop GO-containing composites, which include such matrices as chitosan [36], chitosan-gelatin [37], chitosan-Fe_3O_4 [38] (this composite shows also magnetic properties), carboxymethyl cellulose [39]. These polymers as well as related composites are biodegradable. Among the composites, which can be used repeatedly, the materials that include inorganic ion-exchangers, such as hydrated oxides of multivalent metals, are considered. These compounds are the exclusive inorganic materials: they demonstrate cation and anion exchange properties [40]. Oxides form smaller primary nanoparticles comparing with other ion-exchangers, for instance, phosphate materials [41, 42]. Adsorbents based on hydrated oxides are used for modification of ion exchange resins [43–45], ion exchange membranes [46] and inert porous polymers [41, 42] to enhance their selectivity towards ionic species [43–46] or rejection capability towards colloidal particles [41, 42].

Oxide-based composites containing GO show remarkable functional properties. For instance, the adsorbent that includes double iron-aluminium oxide is highly selective towards As(III) (traditional ion-exchangers cannot be applied, since arsenite salts are not dissociated) [47]. Moreover, the adsorbent based on hydrated zirconium dioxide [48] is capable to remove simultaneously As(III) and As(V) from water. The nanocomposite of MnO_2-GO possesses high selectivity towards Pb(II). Since GO contains both hydrophilic and hydrophobic regions, it is possible to suppose to use the composites also for recovery of organics from water. The aim of this investigation is synthesis of oxide-based GO composite and its testing for adsorption of different species: inorganic ions and organic substances.

EXPERIMENTAL

Finely-dispersed spectrally pure graphite (MG-1) was purchased in «Zaporizhskii graphit» Ltd. GO was obtained by exfoliation of graphite flakes using the improved Hummer's method [50]. A mixture of concentrated H_2SO_4 (360 cm^3) and H_3PO_4 (40 cm^3) was prepared, 3 g of graphite were added to the liquid under stirring. After mixing during 10 min, 18 g of $KMnO_4$ were gradually added into the reaction system that was cooled in ice. The mixture was stirred for 36 h at 50 °C until formation of dark

_____

viscous substance. Then the reaction system was cooled down to room temperature, and transfused slowly into 400 cm^3 of cold deionized water (3 cm^3 of 50 % H$_2$O$_2$ was added to water preliminarily). The suspension was centrifuged and washed subsequently with HCl, water, and methanol up to pH 6. The solid material was collected after centrifugation and dispersed again in 1.2 dm^3 of water. The GO content was determined after drying of 1 cm^3 of the suspension. As found, the content of solid was 2.8 mg·cm^{-3}.

Sol of insoluble zirconium hydroxocomplexes, in which globular nanoparticles (6 nm) and their aggregates dominated, was prepared from a 1 M ZrOCl$_2$ solution similarly to [51]. Sol was stable: no change of particle size over time was found. 90 cm^3 of GO suspension and 100 cm^3 of sol were mixed and treated with ultrasound for 5 min using a Bandelin bath (Bandelin, Hungary). After this, the granules of composite containing hydrated zirconium dioxide (further HZD) and GO were precipitated with a NaOH solution. In alkaline media, GO lost a part of functional groups: additional fragmentation of the particles occurred [52]. Hydrogel obtained by this manner was washed subsequently with NH$_4$OH solution and deionized water up to neutral pH of the effluent, dried at room temperature, and heated at 70 °C down to constant mass. The two-component material (marked further as HZD-GO) contained 20 mg of GO per 1 g of fully dehydrated ZtO$_2$, i.e. approximately 2 % of the carbon filler.

The method of standard contact porosimetry (SCP) [11–13] was used for investigations. First of all, pore size distributions were determined for ceramic standards by means of known techniques of nitrogen adsorption, mercury intrusion, and SEM. Before the measurements of tested sample, it was dried at 150 °C under vacuum, two standards were heated at 170 °C. After heating, both the sample and standards were weighed separately. Then the tested sample was placed between the standards, vacuumized, impregnated with water or octane and dried under vacuum. The set was disassembled from time to time, the sample and standards were weighed. The state of capillary equilibrium was determined for each point of pore size distribution. The measurements were performed to constant mass of the set components. The equilibrium curve of relative moisture content was plotted for the tested sample (amount of liquid in the studied sample *vs* amount of liquid in the standards). Further pore size distributions for the tested sample were plotted. Particle density was determined with the Archimedes technique [53].

FTIR spectra of the samples, which were preliminarily compresses with KBr, were recorded using a Spectrum BX FT-IR spectrometer (PerkinElmer Instruments, USA). Preliminarily the samples of HZD and HZD-GO were regenerated electrochemically using a three-compartment cell similarly to [54]. Electroregeneration was carried out at 90 V. XRD patterns were obtained by means of a DRON-3 spectrometer (Burevestnik, RF) with copper anode and nickel filter. Total cation exchange capacity towards Na$^+$ was determined by treatment of the sample with a 0.1 M NaOH followed by titration of the effluent with a 0.1 M HCl [55].

PbCl$_2$ and NaCrO$_4$ salts were used for preparation of the solutions (0.0001–0.01 mol·dm^3), which were applied to obtaining adsorption isotherms, The solutions were analyzed using a S9 Pye Unicam atomic absorption spectrophotometer (Philips, the Netherlands) at 283.3 (Pb) and 357.9 (Cr) nm. Adsorption capacity was determined from the difference of concentrations before and after adsorption.

The solutions containing phenol (5–70 mg·dm^{-3}) were also prepared. The method of solution analysis before and after adsorption was based on the reaction between phenol, sodium nitroprusside and hydroxylamine hydrochloride in a buffer medium (pH 10.6–11.8) [56].

Adsorption of lactose was also investigated (this disaccharide is a component of the liquid wastes produced by dairy industry). The concentration of this substance was expressed in terms of COD (chemical oxygen demand). Analysis was carried out by oxidation of organics with K$_2$Cr$_2$O$_7$ and H$_2$SO$_4$ followed by titration with Mohr's salt with N-phenylanthranilic acid as an indicator [57].

The adsorption experiments were performed at 25 °C, the dosage of a solid was 0.1 g per 10 cm^3 of a solution.

RESULTS AND DISCUSSION

During precipitation of HZD hydrogel followed by hydrogel-xerogel transformation, rather large granules of adsorbent were formed

(up to 1 mm). The nanoparticles of insoluble zirconium hydroxocomplexes coalesced forming larger particles, a shape of which is close to spheric or elliptic (Fig. 1 *a*). The particles of xerogel ($\approx$ 20–50 nm) are in the form of very compact aggregates. GO nanoparticles ($\approx$ 2–3 nm) are also aggregated (Fig. 1 *b*). The shape of aggregates is irregular, their size is 30–100 nm. As known, GO aggregates form agglomerates of micron size, this information is available elsewhere, for instance, in [37].
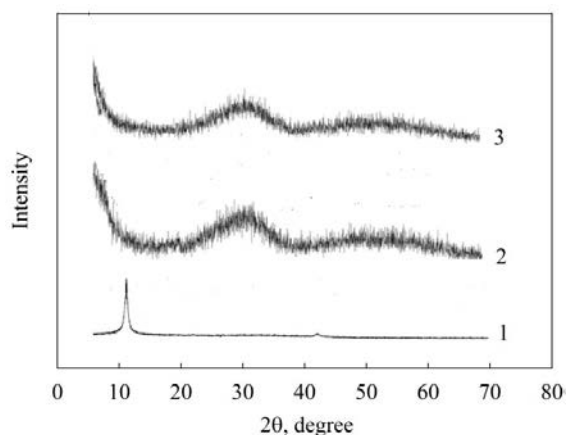

a

b

c

d

e
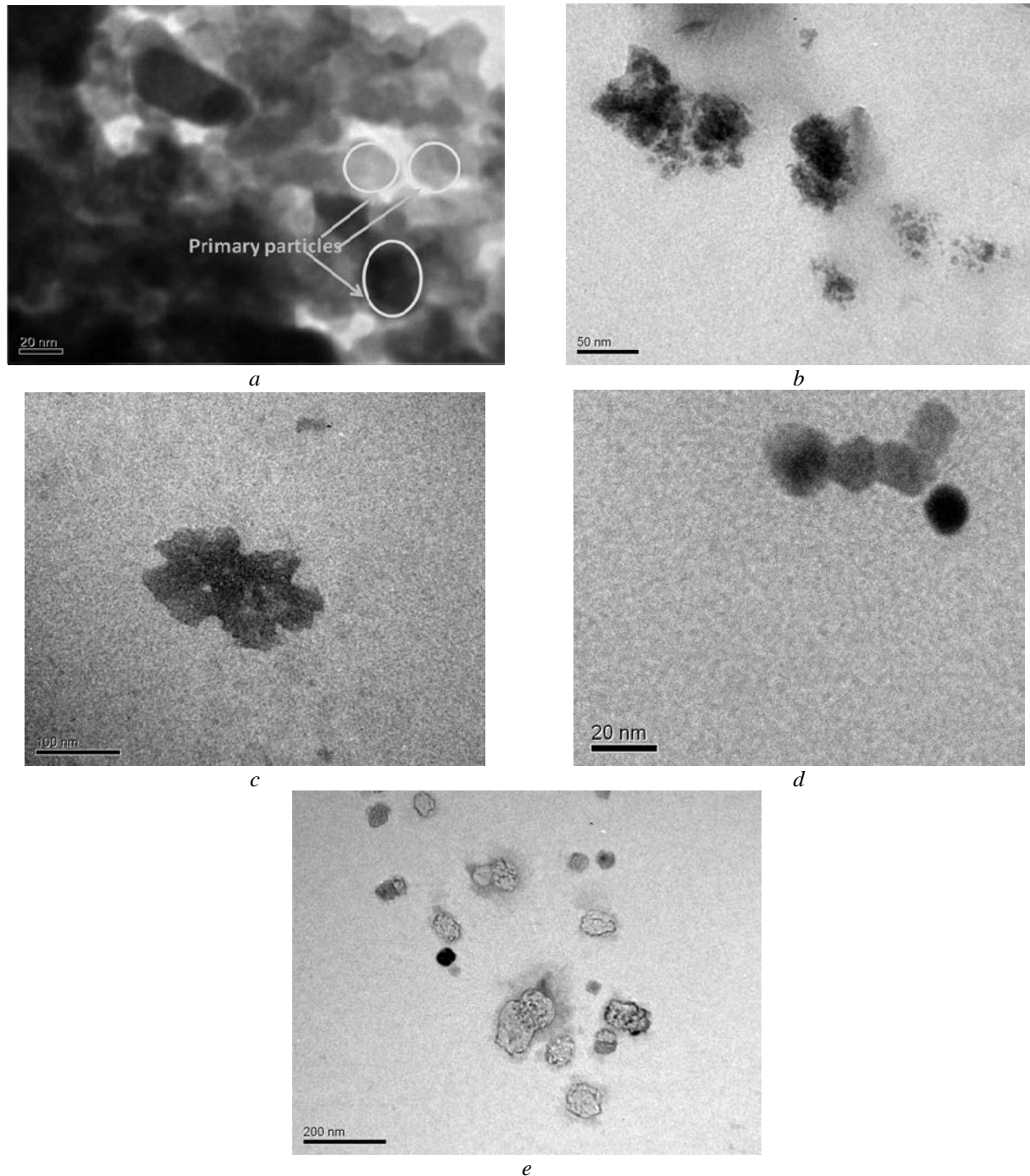
Fig. 1. TEM images of HZD (*a*), GO (*b*) and two-component material (*c–e*). HZD surface is covered with GO nanoparticles (*c*) and free from GO (*d*), traces of GO aggregates after chemical transformation of carbon affected by accelerated electrons of microscope (*e*)

In the case of two-component material, HZD structure is evidently more friable comparing with one-component inorganic adsorbent (Fig. 1 *c*). This gives a possibility to observe individual aggregates in TEM images. Similarly to pure HZD, the globules of sol coalesced to larger particles (up to 50 nm) during hydrogel deposition. In turn, these particles formed elliptic splices (up to 150 nm) with uneven edges. As seen, GO nanoparticles are distributed on the HZD surface. Under the action of accelerated electrons of the microscope, graphene structure is destroyed, further carbon is redeposited onto copper substrate, when the sample is placed. Nanosized bubbles are formed (they are seen as white spots).

Chains of fused spherical and elliptic HZD nanoparticles (≈ 20 nm) have been also found (Fig. 1 *d*). Their surface is free from GO probably due to its small content. The material includes also GO aggregates (50–150 nm), which are not associated with HZD surface. Their traces after chemical transformation of carbon are seen in Fig. 1 *e*. Thus, the HZD-GO sample consists of HZD particles, which are partially covered with GO, and GO aggregates.

Fig. 2 illustrates the XRD patterns of GO, HZD and HZD-GO. In the case of GO, typical peak at 11.41° is visible. This signal is attributed to the (001) reflection of GO and corresponds to the distance between layers of 7.68 Å [58]. Regarding HZD, the peak is blurred indicating amorphous structure. Similar result was obtained for the two-component material: the typical GO reflex is invisible evidently due to small content of the carbon filler in the inorganic matrix.

The data of FTIR spectroscopy are given in Fig. 3. The spectra for all samples show very broad peaks in the region of 3100–3400 cm^{-1}: these bands are attributed to OH vibrations of adsorbed water molecules. Regarding GO, several peaks are visible, they are related to stretching vibration of C–O–C (epoxy groups, 1070 cm^{-1}), C–OH (hydroxyl and carboxyl groups, 1257 cm^{-1}), O=C–OH (carboxyl groups, 1401 cm^{-1}), C–C (aromatics, i.e. carbon skeletal network, 1620 cm^{-1}), C=O (carbonyl of carboxyl groups, 1722 cm^{-1}) [58].
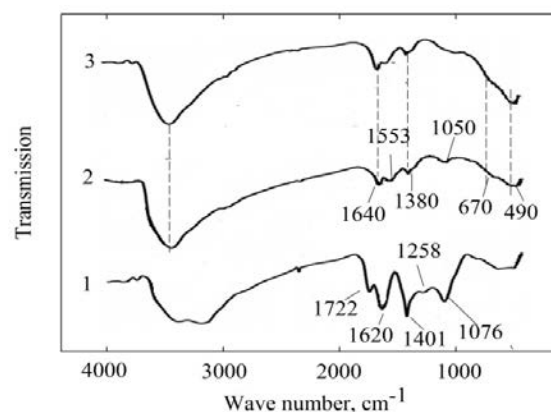
Fig. 3. FTIR spectra of GO (*1*), HZD (*2*) and HZD-GO (*3*)

The spectrum of HZD demonstrates following peaks that correspond to stretching vibrations: Zr–O (Zr–OH surface groups, 490 cm^{-1}), Zr–O–Zr (bulk of primary particles, broad band at 550–750 cm^{-1}), Zr–OH (1380, 1553 cm^{-1}), and O–Zr–OH (1640 cm^{-1}) [59]. The band at 1050 cm^{-1} is evidently attributed to deformation vibration of Zr–O–H fragments. Formation of Zr–O–Zr bonds occurs during hydrogel-xerogel transformation, these bonds cause coalescence of particles, and provide compactness of HZD xerogel.

In the case of two-component material, no bands attributed to GO has been found. The spectrum shows the peaks, which are characteristic to hydrated metal oxide. No shifts of bands and no additional peaks mean different phases of HZD and GO indicating no formation of new types of bonds or destruction of existing bonds.

This composition of HZD-GO affects its porous structure, as shown in Table 1 and Fig. 4. First of all, GO is characterized by high microporosity and large specific surface area.

Fig. 2. XRD patterns of GO (*1*), HZD (*2*) and two-component material (*3*)

_____

The MSCP gives much higher values comparing with BET method [9, 10], since octane provides disjoining pressure, wets GO sheets completely penetrating between them. In the case of water medium, the extension of graphene sheets is caused by hydration of functional groups. As opposed to [13], larger microporosity and specific surface area were obtained in aqueous medium. It means, GO behaves similarly to ion exchange polymers at the level of micropores [60]. This is evidently due to hydration of functional groups followed by GO swelling. At the same time, porosity in octane is higher than that in water due to significant contribution of hydrophobic meso- and macropores.

Addition of small amount of GO to HZD significantly decreases particle density of the inorganic matrix (16 %). This indicates higher content of −OH groups per unit of area of inorganic surface (note that the surface area increases insufficiently for HZD-GO comparing with HZD). Indeed, a total ion exchange capacity (towards Na^+) is 1.16 mmol·g^{-1} (HZD) and 1.30 mmol·g^{-1} (HZD-GO). In the case of GO, this value is 1.05 mmol g^{-1}. At the same time, the growth of content of functional groups enhances hydration of HZD surface: water associated with the surface cannot be removed completely during thermal pretreatment at 150 °C. Mass losses are only 8.3 (HZD) and 11.7 % (HZD-GO) under these conditions. Thus, the increase of content of −OH groups and bonded water provides reducing particle density, which is determined by Archimedes method.

Table 1. Data of porometric measurements

Sample	Working liquid	Particle density, g cm^{-3}	Total porosity	Micropores, $cm^3 g^{-1}$	Surface area, $m^2 g^{-1}$		
					total	micropores	meso- and macropores
HZD	water	5.07	0.73	0.19	382	379	2
GO	water		0.85	0.45	2250	900	1350
	octane	1.81	0.95	0.23	1200	460	740
HZD+GO	water		0.67	0.19	391	381	10
	octane	4.24	0.66	0.17	363	350	13

The composite shows slight reducing total porosity, microporosity remains the same. As opposed to GO and similarly to HZD, micropores make main contribution to the surface area.

Integral pore volume distributions, which were obtained both in water and octane media, are plotted in Fig. 4 *a*, *b* as dependences of pore volume (*V*) on logarithm of effective pore radius (*r**) [11–13]. The *r** term is applied to the materials containing both hydrophilic and hydrophobic pores, this value corresponds to:

$$r^* = r \cdot \sec\theta, \tag{1}$$

where *θ* is the wetting angle. In fact, the experimental curves for hydrophilic-hydrophobic materials are *V*− *r** dependences. Both hydrophilic and hydrophobic pores (total porosity) are determined with octane that wets all materials ideally. Here $\cos\theta = 1$, *r** = *r*, where *r* is the true pore radius. Water is used for recognition of hydrophilic pores. For completely hydrophilic materials like HZD, *r** = *r*. Regarding hydrophilic-hydrophobic materials, the experimental *V*− *r** distributions are shifted towards larger *r** values relatively to the curve obtained in octane medium. This shift is observed in most cases.

Figs. 4 *c–d* illustrate differential distributions. Since the equality of

$$\int_{\log r_2^*}^{\log r_2^*} \frac{dV}{d(\lg r^*)} d(\lg r^*) = \int_{lr_1^*}^{r_2^*} \frac{dV}{dr^*} dr^*$$ is valid, the

area of each peak corresponds to a contribution of certain pores to total porosity,

$$\frac{dV}{d(\lg r^*)} = 2.3 r^* \frac{dV}{dr^*}.$$

HZD is characterized by compact structure: this adsorbent is practically non-porous within the *r** interval of 1 nm – 2 μm: only a small peak is visible at *r**=1.5 nm. This confirms SEM data (see Fig. 1 *a*). Only micropores (intersection of integral curves with ordinate axes) and

macropores ($r* > 2\,\mu$m) contribute to porosity. At $r* > 15\,\mu$m, the effect of voides between granules is observed, this interval is outside the focus of our attention.

As opposed to completely hydrophilic HZD, GO contains both hydrophilic and hydrophobic regions. In contrast to ordinary carbon materials [11–13], the $V - r*$ distribution for water medium is shifted towards lower $r*$ values relatively the curve obtained in octane ($r* < 2\,\mu$m). It is typical for ion exchange membranes [60], which demonstrate strong swelling in water, or carbon paper for gas-diffusion layer of fuel cells [61]. This «superhydrophilicity» is caused for hydration of functional groups. Formally, $\cos\theta = 0$ in this region due micropores, which are evidently attributed to the voids between primary nanoparticles. Micropores are mainly hydrophilic. The region at 10–100 nm is related to hydrophilic pores caused by the interstices between aggregates. These pores are rather regular in octane medium: the half-width of apparent peak is 15 nm ($r* = 10$–30 nm and 50–80 nm). Hydration of the GO surface results in broadening the peaks.

Starting at $r* = 2\,\mu$m, hydrophobic pores dominate in GO. These macropores are attributed to agglomerates of micron size, curing of sheets *etc*. Thus, the pores caused by nanosized fragments and their aggregates are hydrophilic. At the same time, the voids between agglomerates are hydrophobic. It means, aggregation is due to formation of hydrogen bonds between functional groups along the particles (Fig. 5). On the contrary, agglomerates are formed by hydrophobic regions. This is probably due to involvement of hydrophilic regions in aggregate formation.

As opposed to HZD, the HZD-GO sample is characterised by developed pores in the interval of $r* = 3$ nm–1.5 μm (see Figs. 1 *a, c, d*). The integral distributions, which were obtained in different media, are rather close to each other due to the effect of hydrophilic inorganic matrix. However, the volume of hydrophilic pores is higher than that obtained in octane. This is observed within the interval of $r* = 1$ nm–100 μm. In other words, this interval is much wider comparing with GO. The regular peaks at 20 (water) and irregular maximum at 50 (octane) nm are evidently due to the carbon filler. This is

confirmed by different positions of the maxima, and by correspondence to the curves for the individual GO.

Regarding the integral curve, which was obtained using water, the build-up is 0.1 cm^3·g^{-1} at $r* = 1$–100 nm. The growth of 6 cm^3·g^{-1} is for GO in this region. It means 1.5 mass. % of GO in the composite. Similar ratio for the curves obtained in octane medium gives 2.3 mass. % of GO (0.7 cm^3·g^{-1} for HZD-GO and 3 cm^3·g^{-1} for GO). The composite contained ≈ 2 mass. % of GO. Thus, the results are close to reality indicating significant contribution of GO into porosity at $r* = 1$–100 nm. Further the pore size distribution for water medium shows plateau up to 10 μm (GO) or growth up to 1.5 μm (HZD-GO). This means, the region of $r* > 100$ nm is related mainly to HZD aggregates. However, the volume of «water» pores is larger comparing with «octane» voids. This shows coverage of large HZD particles with GO sheets. The adsorbed sheets of the carbon material prevent compaction of HZD particles through Zr–O–Zr bonds. Thus, at the level of macropores (100 nm – 10 μm), porous structure of the HZD constituent is much more developed comparing with pure HZD.

Let us note also higher ratio of volumes of pores, which are recognized by water and octane ($r* = 1$–100 nm), for the HZD-GO sample comparing with pure GO. Thus, GO sheets are associated with HZD surface by means of hydrophilic fragments. As a result, these fragments are excluded from formation of pores of mentioned size. This is accompanied by enhancing hydrophobicity.

GO sheets are associated with HZD surface through hydrogen-bonding and Lewis acid-base interactions (the π-electron system of graphite planes acts as Lewis basic sites) [62]. When the solution pH is lower than point of zero charge of oxide (positive charge of the matrix surface), but higher than 3 (dissociation of –COOH groups of GO, negative charge of carbon surface), these interactions are enhanced by electrostatic attraction [18].

In general, the structure of HZD and HZD-GO can be represented schematically (Fig. 6). The inorganic adsorbent is characterized by compact structure, GO sheets partially screen the surface of HZD particles making impossible their compactness. This provides more friable

structure of the composite comparing with pure HZD. However, some HZD particles are free from GO (see Fig. 1 *d*). This allows one partial linkage of HZD through Zr–O–Zr bonds. The linkage prevents fragmentation of granules in a solvent.
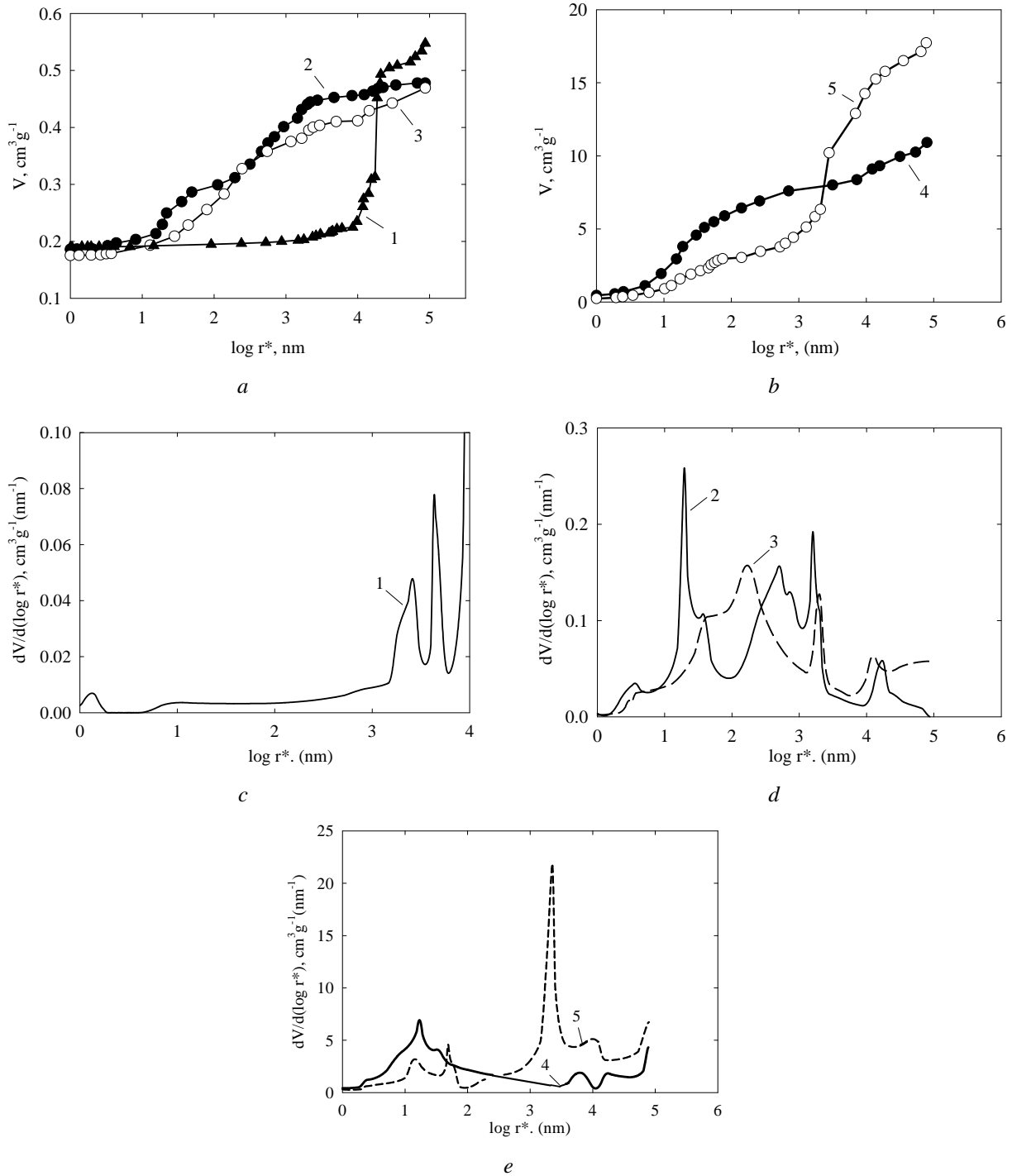
Fig. 4. Integral (*a, b*) and differential (*c-e*) pore size distributions obtained for HZD (*1*), composite (*2, 3*) and GO (*4, 5*). Working liquid is water (*1, 2, 4*) or octane (*3, 5*)

a

b
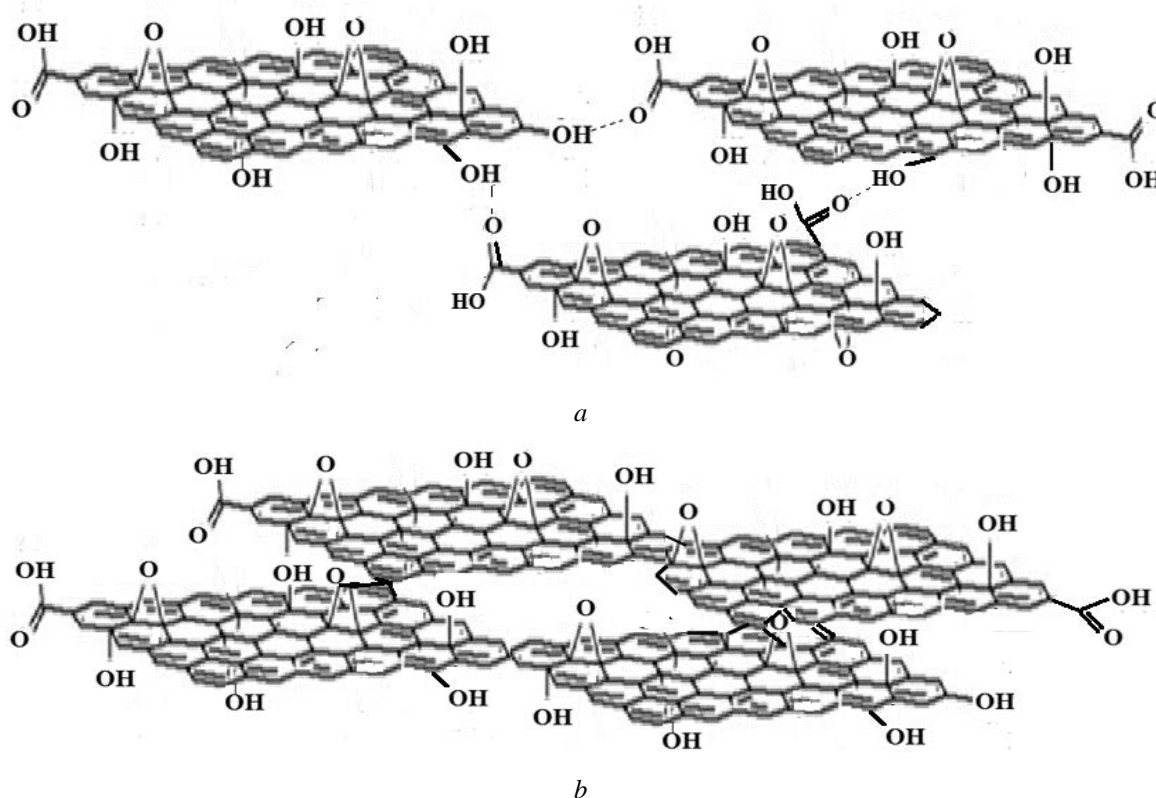
Fig. 5. Formation of hydrophilic (*a*) and hydrophobic (*b*) pores due to aggregates and agglomerates respectively. Only fragments of aggregates and agglomerates are shown for clarity

Insertion of GO into HZD affects functional properties of the inorganic material, for instance, the capability to sorb inorganic cations and anions. In the case of adsorption of Pb(II) and Cr(VI)-containing ions, the pH of equilibrium solutions slightly shifted to acidic region. Thus, it is possible to say about $HCrO_4^-$ adsorption. The pH shift is due to Pb(II)$\rightarrow$H$^+$ or Na$^+\rightarrow$ H$^+$ exchange (since HZD is amphoteric, cations of chromate salt are also adsorbed).

The isotherm of Pb(II) adsorption on GO is characterized by a rapid build-up in the field of low equilibrium concentrations (*C*) followed by plateau (Fig. 7 *a*). In the case of HZD, the growth of adsorption capacity (*A*) is much slower, the tendency to plateau is visible in the region of high concentrations. In comparison with HZD, the isotherm for HZD-GO shows a steeper ascent. Adsorption capacity of the composite is higher in 1.7 times evidently due to GO contribution. At the same time, GO in the composite depresses $HCrO_4^-$ adsorption: this is caused by screening of adsorption centers on the

HZD surface. No adsorption of chromate ions on GO was found, this was due to the absence of anion exchange groups.

The Langmuir model can be applied to the isotherms in accordance to equation [63]:

$$\frac{1}{A} = \frac{1}{K_L A_L C} + \frac{1}{A_L}, \qquad (2)$$

where *C* is the equilibrium concentration, A_∞ is the monolayer capacity, *K* is the constant that characterizes energy of interaction with surface. The A_∞ values were determined also from the original data by extrapolation of the isotherms to infinity (Fig. 8 *b*). The experimental and calculated A_∞ magnitudes are close to each other indicating validity of the Langmuir model for ion adsorption (Table 2). The HZD-GO sample demonstrates intermediate A_∞ and *K* constants (between HZD and GO) for Pb(II) adsorption isotherm. Regarding $HCrO_4^-$ adsorption, the constants are lower for the composite comparing with pure HZD.

_____
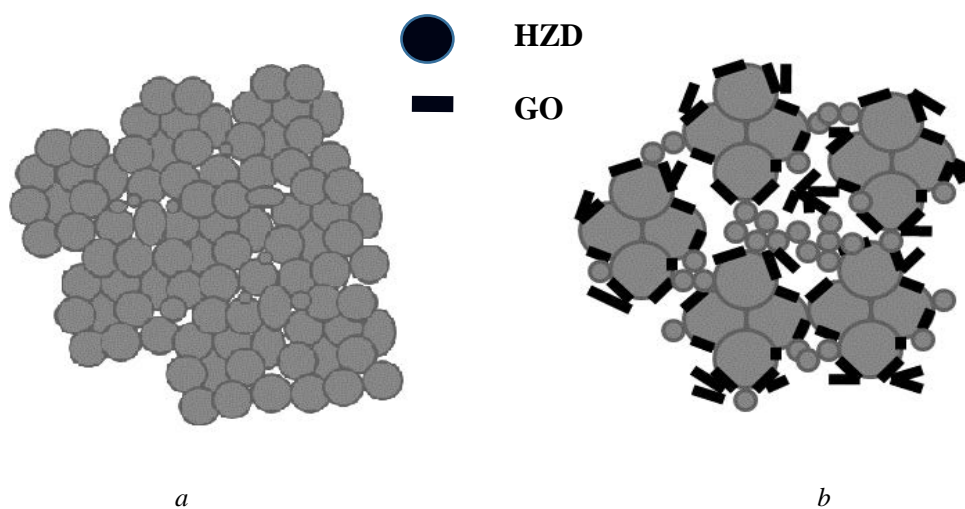
Fig. 6. Schematic image of HZD (*a*) and HZD-GO (*b*) structure in a solvent
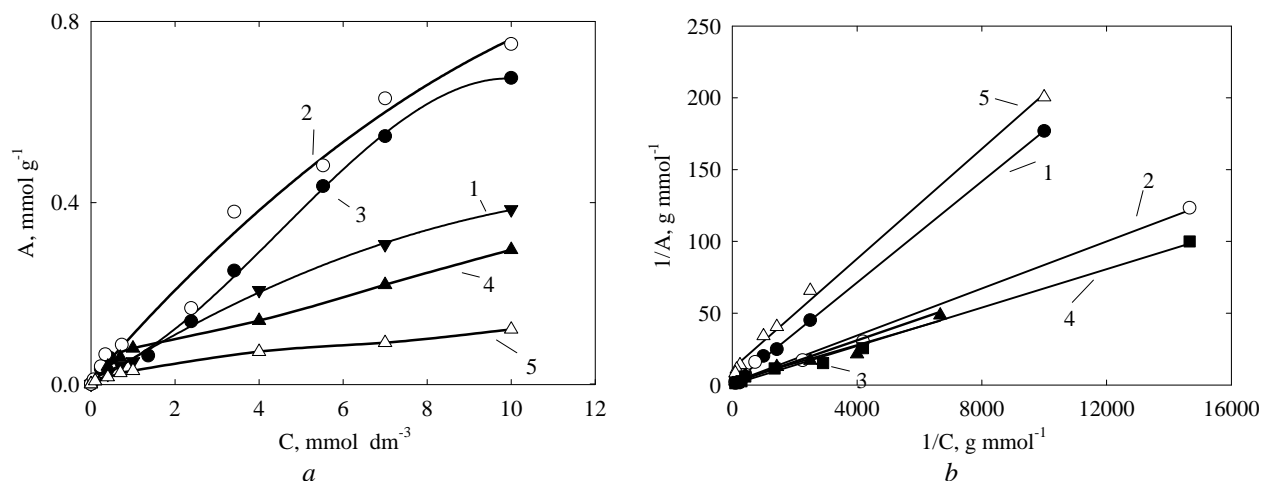
Fig. 7. Isotherms of Pb(II) (*1–3*) and HCrO$_4^-$ (*4, 5*) adsorption on HZD (*1, 4*), GO (*2*) and HZD-GO (*3, 5*) in common and Langmuir coordinates

Table 2. Application of Langmuir model to adsorption of Pb(II) and HCrO$_4^-$ ions

Sample	Removal degree, %		A∞, mmol g^{-1}		K, g mmol^{-1}	R^2
	maximal	minimal	experimental	calculated according to the model		
Pb(II)						
HZD	56	38	0.51	0.58	37	0.99
GO	99	75	1.46	1.33	279	0.99
HZD- GO	81	67	0.86	0.81	217	0.98
HCrO$_4^-$						
HZD	67	33	0.53	0.64	233	0.98
HZD- GO	63	12	0.17	0.10	175	0.99

Despite depressed anion exchange properties, the composite adsorbs phenol that is a weak acid (Table 3). When the initial concentration of this component is 5 mg dm^{-3}, the HZD-GO sample removes it down to maximal allowable concentration for tap water (1 µg·dm^{-3}). Adsorption is due to hydrophobic regions of GO sheets. Indeed, pure GO sorbs phenol very efficiently. In the case of one-component HZD, adsorption of phenol is inconsiderable.

The composite is also effective towards such molecular substance as lactose. It allows one to reach the COD value that is lower than the maximal allowable concentration for tap water (5 mg·dm^{-3}). Conversely, HZD shows no adsorption of lactose.

Table 3. Removal of organics from water

Sample	Initial concentration (phenol) or COD (lactose), mg dm^{-3}	Residual concentration (phenol) or COD (lactose), µg dm^{-3}	Removal degree, %
		phenol	
HZD	5	4700	6
	21	20500	2
	70	69000	1
GO	5	<1	100
	21	<1	100
	70	4	99
HZD- GO	5	<1	100
	21	30	99
	70	420	99
		lactose	
HZD		55	0
GO	55	1	98
HZD- GO		3	94

CONCLUSIONS

The composite that includes HDZ and ≈ 2 mass. % of GO has been synthesized by deposition from sol containing dispersed particles of the filler. The composite includes HZD particles covered with GO sheets, uncovered particles, free and agglomerated GO. Mechanical strength of granules are due to uncovered HZD particles.

As opposed to BET method, the MSCP gives high specific surface area of GO in octane: this solvent wets ideally the sheets penetrating between them. Much higher value of surface area for water medium is caused by hydration of functional groups followed by swelling of GO. This behavior is similar to ion exchange polymers. The filler provides loosening of HZD within a wide interval of pore size.

The filler improves adsorption of Pb(II) ions increasing the capacity in 1.7 times due to its expressed cation exchange properties. Contrary, GO depresses adsorption of HCrO$_4^-$ anions. The composite is effective towards weakly acidic phenol and molecular organic substance, such as lactose. Possible fields of the composite application is water purification and water processing.

The main direction of further investigations are composition control for multifunctional composites, which would provide both high adsorption capability and mechanical strength of granules. It is also desirable to replace the inorganic matrix to cheaper material, to ascertain the possibility of multiple usage of adsorbents. The modification with GO is expected to be efficient for modifying of other inorganic cation-exchangers, which could be easy regenerated with acids without destruction. At last, the composite can be proposed for modification of membranes similarly to HZD [41, 42, 51] or carbon materials [64, 65].

Композит, який складається з гідратованого діоксиду цирконію та оксиду графену, для вилучення органічних та неорганічних компонентів з води

**Ю.С. Дзязько, В.М. Огенко, Ю.М. Вольфкович, В.Е. Сосєнкін,
Т.В. Мальцева, Т.В. Яценко, К.О. Куделко**

*Інститут загальної та неорганічної хімії ім. В.І. Вернадського Національної академії наук України
просп. Академіка Палладіна, 32/34, Київ, 03680, Україна, dzyazko@gmail.com
Інститут фізичної хімії та електрохімії ім. О.Н. Фрумкіна Російської академії наук
Ленінський пр., 31, Москва, 119071, Росія, yuvolf40@mail.ru*

Мета роботи полягала у розробці багатофункціонального адсорбента, який здатний видаляти з водних розчинів як неорганічні іони, так і молекулярні органічні сполуки. Окиснений графен отримано методом Хаммера. Композит, який включає гідратований діоксид цирконію та оксид графену (≈ 2 мас. %), був синтезований осадженням із золю, що містив дисперсні частинки вуглецевого матеріалу. Адсорбент та його складові досліджено методами рентгенофазового аналізу, ІЧ-Фур'є спектроскопії, ТЕМ та еталонної контактої порометрії при застосуванні води та октану як робочих рідин. Виявлено сильну гідратацію оксиду графену у воді: об'єм мікро- та мезопор у водному середовищі є набагато вищим, ніж в октані. Це вказує на аналогічну поведінку графену та іонообмінних полімерів. Це, вочевидь, пов'язано з гідратацією його функціональних груп (гідроксильних, карбоксильних та епоксигруп). Для оксиду графену виявлено великі значення площі питомої поверхні, які досягають 1200 (в органічному розчиннику) або 2250 $м^2г^{-1}$ (у воді). Показано, що графен вкриває частинки неорганічної матриці, розпушуючи її в широкому інтервалі розмірів пор (від 10 нм до 1.5 мкм). Як виявлено, ізотерми адсорбції іонів Pb(II) та $HCrO_4^-$ відповідають моделі Ленгмюра. Завдяки вираженим катіонообмінним властивостям, наповнювач покращує адсорбцію іонів Pb(II), збільшуючи ємність у 1.7 рази. Навпаки, аніонообмінна функція композиту пригнічується, оскільки шари оксиду графену екранують адсорбційні центри неорганічної матриці. Іншою причиною може бути електростатичне відштовхування аніонів, адже точка нульового заряду композиту зсувається до кислої області. Завдяки вуглецевому наповнювачу оксидний матеріал набуває спроможності адсорбувати як слабкодисоційовані (фенол), так і молекулярні (лактоза) органічні сполуки. Якщо початкова концентрація фенолу становить 5 мг дм$^{-3}$, можливо знизити його вміст у воді до гранично припустимої концентрації. Після адсорбції вміст лактози у розчині є набагато меншим цього параметра. Таким чином, композит забезпечує практично повне видалення органіки з води.

Ключові слова: *оксид графену, гідратований діоксид цирконію, еталонна контактна порометрія, гідрофільні пори, гідрофобні пори, адсорбція, свинець, хромат, фенол, лактоза*

Композит, состоящий из гидратированного диоксида циркония и оксида графена, для извлечения органических и неорганических компонентов из воды

**Ю.С. Дзязько, В.М. Огенко, Ю.М. Вольфкович, В.Е. Сосенкин,
Т.В. Мальцева, Т.В. Яценко, Е.О. Куделко**

*Институт общей и неорганической химии им. В.И. Вернадского Национальной академии наук Украины
просп. Академика Палладина, 32/34, Киев, 03680, Украина, dzyazko@gmail.com
Институт физической химии и электрохимии им. А.Н. Фрумкина Российской академии наук
Ленинский пр. 31, Москва, 119071, Россия, yuvolf40@mail.ru*

Цель работы заключалась в разработке многофункционального адсорбента, который способен удалять из водных растворов как неорганические ионы, так и молекулярные органические соединения. Окисленный графен получали по методу Хаммера. Композит, включающий гидратированный диоксид циркония и оксид графена (≈ 2 мас. %) синтезирован осаждением из золя, содержащего дисперсные частицы углеродного материала. Адсорбент и его составляющие исследованы методами рентгенофазового анализа, ИК-Фурье спектроскопии, ТЭМ и эталонной контактной порометрии при использовании воды и октана в качестве

_____

рабочих жидкостей. Обнаружено сильную гидратацию оксида графена в воде: объем микро и мезопор в водной среде намного больше, чем в октане. Это указывает на аналогичное поведение графена и ионообменных полимеров. Данный факт обусловлен гидратацией его функциональных групп (гидроксильных, карбоксильных, эпоксигрупп). Для оксида графена найдены высокие значения площади удельной поверхности, которые достигают 1200 (в органическом растворителе) или 2250 $м^2г^{-1}$ (в воде). Показано, что графен покрывает частицы неорганической матрицы, разрыхляя ее в широком интервале размеров пор (от 10 нм до 1.5 мкм). Как обнаружено, изотермы адсорбции ионов Pb(II) и $HCrO_4^-$ соответствуют модели Ленгмюра. Благодаря выраженным катионообменным свойствам наполнитель улучшает адсорбцию ионов Pb(II), увеличивая емкость в 1.7 раза. Напротив, анионообменная функция композита подавляется, поскольку слои оксида графена экранируют адсорбционные центры неорганической матрицы. Другой причиной может быть электростатическое отталкивание анионов, поскольку точка нулевого заряда композитов смещается в кислую область. Благодаря углеродному наполнителю, оксидный материал приобретает способность адсорбировать как слабодиссоциированные (фенол), так и молекулярные (лактоза) органические соединения. Если начальная концентрация фенола составляет 5 мг дм$^{-3}$, возможно снизить его содержание в воде до предельно допустимой концентрации. После адсорбции концентрация лактозы в растворе намного меньше этого параметра. Таким образом, композит обеспечивает практически полное удаление органики из воды.

Ключевые слова: *оксид графена, гидратированный диоксид циркония, эталонная контактная порометрия, гидрофильные поры, гидрофобные поры, адсорбция, свинец, хромат, фенол, лактоза*

REFERENCES

1. Young R.J., Kinloch I.A., Gong L., Novoselov K.S. The mechanics of graphene nanocomposites: A review. *Compos. Sci. Technol.* 2012. **72**(12): 1459.
2. Choi Y.R., Yoon Y.-G., Choi K.S., Kang J.H., Shim Y.-S., Kim Y.-H., Hye Jung Chang H.J., Lee J.-H., Park Ch.R., Kim S.Y., Jang H.W. Role of oxygen functional groups in graphene oxide for reversible room-temperature NO$_2$ sensing. *Carbon*. 2015. **91**: 178.
3. Chabot V., Higgins D., Yu A., Xiao X., Chen Z., Zhang J. A review of graphene and graphene oxide sponge: material synthesis and applications to energy and the environment. *Energy Environ. Sci.* 2014. **7**: 1564.
4. Zhu Y., Murali Sh., Cai W., Li X., Suk J.W., Potts J.R., Ruof R.S. Graphene and Graphene Oxide: Synthesis, Properties, and Applications. *Adv. Mater.* 2010. **22**(35): 3906.
5. Dreyer D.R., Park S., Bielawski C.W., Ruoff R.S. The chemistry of grapheme oxide. *Chem. Soc. Rev.* 2010. **39**(1): 228.
6. Chen D., Feng H., Li J. Graphene oxide: preparation, functionalization, and electrochemical Applications. *Chem. Rev.* 2012. **112**(11): 6027.
7. Barbolina I., Woods C.R., Lozano N., Kostarelos K., Novoselov K.S., Roberts I.S. Purity of graphene oxide determines its antibacterial activity. *2D Mater.* 2016. **3**(2): 025025.
8. Chen Ch.-H, Hu Sh., Shih J.-F., Yang Ch.-Y., Luo Y.-W., Ren-Huai Jhang R.-H., Chiang Ch.-M., Hung Y.-J. Effective synthesis of highly oxidized graphene oxide that enables wafer-scale nanopatterning: preformed acidic oxidizing medium approach. *Sci. Rep.* 2017. **7**: 3908.
9. Seresht R.J., Jahanshahi M., Rashidi A., Ghoreyshi A.A. Synthesize and characterization of graphene nanosheets with high surface area and nano-porous structure. *Appl. Surf. Sci.* 2013. **276**: 672.
10. McAllister M.J., Li J.-L., Adamson D.H., Schniepp H.C, Abdala A.A., Liu J., Herrera-Alonso M., Milius D.L., Car R., Prud'homme R.K., Aksay I.A. Single sheet functionalized graphene by oxidation and thermal expansion of graphite. *Chem. Mater.* 2007. **19**(18): 4396.
11. Volfkovich Yu.M., Sosenkin V.E. Porous structure and wetting of fuel cell components as the factors determining their electrochemical characteristics. *Russ. Chem. Rev.* 2012. **86**(6): 936.
12. Volfkovich Yu.M., Bagotsky V.S. Experimental methods for investigation of porous materials and powders, In: *Porous materials and powders used in different fields of science and technology.* (London: Springer-Verlag, 2014).
13. Volfkovich Y.M., Rychagov A.Y., Sosenkin V.E., Efimov O.N., Os'makov M.I. Measuring the specific surface area of carbon nanomaterials by different methods. *Russ. J. Electrochem.* 2014. **50**(11): 1099.
14. Rouquerol J., Baron G., Denoyel R., Giesche H., Groen J., Klobes P., Levitz P., Neimark A.V., Rigby S., Skudas R., Sing K., Thommes M., Unger K. Liquid intrusion and alternative methods for the characterization of macroporous materials (IUPAC Technical Report). *Pure Appl. Chem.* 2012. **84**(1): 107.

_____

15. Xu Z., Sun H., Zhao X., Gao Ch. Ultrastrong fibers assembled from giant graphene oxide sheets. *Adv. Mater.* 2012. **25**(2): 188.

16. Paredes J.I., Villar-Rodil S., Martínez-Alonso A., Tascón J.M.D. Graphene oxide dispersions in organic solvents. *Langmuir.* 2008. **24**(19): 10560.

17. Dikin D.A., Stankovich S., Zimney E.J., Piner R.D., Dommett G.H.B., Evmenenko G., Nguyen S.T., Ruoff R.S. Preparation and characterization of graphene oxide paper. *Nature.* 2007. **448**: 457.

18. Sheng G., Huang Ch., Chen G., Sheng J., Ren X., Hu B., Ma J., Wang X., Huang Y., Alsaedi A., Hayat T. Adsorption and co-adsorption of graphene oxide and Ni(II) on iron oxides: A spectroscopic and microscopic investigation. *Environ. Pollut.* 2018. **233**: 125.

19. Sotirelis N.P., Chrysikopoulos C.V. Interaction between graphene oxide nanoparticles and quartz sand. *Environ. Sci. Technol.* 2015. **49**(22): 13413.

20. Chrysikopoulos C.V., Sotirelis N.P., Kallithrakas-Kontos N.G. Cotransport of graphene oxide nanoparticles and kaolinite colloids in porous media. *Transp. Porous Media.* 2017. **119**(1): 181.

21. Sotirelis N.P., Chrysikopoulos C.V. Heteroaggregation of graphene oxide nanoparticles and kaolinite colloids. *Sci. Total Environ.* 2017. **579**: 736.

22. Chen Ch., Shang J., Zheng X., Zhao K., Yan Ch., Sharma P., Liu K. Effect of physicochemical factors on transport and retention of graphene oxide in saturated media. *Environ. Pollut.* 2018. **236**: 168.

23. Wang J., Yao W., Gu P., Yu Sh., Wang X., Du Y., Wang H., Zhongshan Chen Z., Hayat T., Wang X. Efficient coagulation of graphene oxide on chitosan–metal oxide composites from aqueous solutions. *Cellulose.* 2017. **24**(2): 851.

24. Liu X., Li J., Huang Y., Wang X., Zhang X., Wang X. Adsorption, aggregation, and deposition behaviors of carbon dots on minerals. *Environ. Sci. Technol.* 2017. **51**(11): 6156.

25. Hongwen L.S., Fugetsu Y.B. Graphene oxide adsorption enhanced by *in situ* reduction with sodium hydrosulfite to remove acridine orange from aqueous solution. *J. Hazard. Mater.* 2012. **203-204**: 101.

26. Zhang W., Zhou Ch., Zhou W., Lei A., Zhang Q., Wan Q., Zou B. Fast and considerable adsorption of methylene blue dye onto graphene oxide. *Bull. Environ. Contam. Toxicol.* 2011. **87**(1): 86.

27. Ramesha G.K., Kumara A.V., Muralidhara H.B., Sampath S. Graphene and graphene oxide as effective adsorbents toward anionic and cationic dyes. *J. Colloid Interface Sci.* 2011. **361**(1): 270.

28. Gao Y., Li Y., Zhang L., Huang H., Hu J., Shah S.M., Su X. Adsorption and removal of tetracycline antibiotics from aqueous solution by graphene oxide. *J. Colloid Interface Sci.* 2012. **368**(1): 540.

29. Pavagadhi S., Tang A.L.L., Sathishkumar M., Loh K.P., Balasubramanian R. Removal of microcystin-LR and microcystin-RR by graphene oxide: Adsorption and kinetic experiments. *Water Res.* 2013. **47**(13): 4621.

30. Wu M., Kempaiah R., Huang P.-J.J., Maheshwari V., Liu J. Adsorption and desorption of DNA on graphene oxide studied by fluorescently labeled oligonucleotides. *Langmuir.* 2011. **27**(6): 2731.

31. Wang J., Chen Z., Chen B. Adsorption of polycyclic aromatic hydrocarbons by graphene and graphene oxide nanosheets. *Environ. Sci. Technol.* 2014. **48**(9): 4817.

32. Zhao G., Li J., Ren X., Chen Ch., Wang X. Few-layered graphene oxide nanosheets as superior sorbents for heavy metal ion pollution management. *Environ. Sci. Technol.* 2011. **45**(24): 10454.

33. Sitko R., Turek E., Zawisza B., Malicka E., Ewa Talik E., Jan Heimann J., Gagor A., Feist B., Wrzalik R. Adsorption of divalent metal ions from aqueous solutions using graphene oxide. *Dalton Trans.* 2013. **42**: 5682.

34. Tan P., Sun J., Hu Y., Fang Z., Bi Q., Chen Y., Cheng J. Adsorption of Cu^{2+}, Cd^{2+} and Ni^{2+} from aqueous single metal solutions on graphene oxide membranes. *J. Hazard. Mater.* 2015. **297**: 251**.**

35. Li Z., Chen F., Yuan L., Liu Y., Zhao Y., Chai Z., Shi W. Uranium(VI) adsorption on graphene oxide nanosheets from aqueous solutions. *Chem. Eng. J.* 2012. **210**: 539.

36. Li L., Li C., Bao Ch., Jia Q., Xiao P., Liu X., Zhang Q. Preparation and characterization of chitosan/graphene oxide composites for the adsorption of Au(III) and Pd(II). *Talanta.* 2012. **93**: 350.

37. Zhang N., Qiu H., Si Y., Wang W., Gao J. Fabrication of highly porous biodegradable monoliths strengthened by graphene oxide and their adsorption of metal ions. *Carbon.* 2011. **49**(3): 827.

38. Fan L., Ch., Sun M., Li X., Qiu H. Highly selective adsorption of lead ions by water-dispersible magnetic chitosan/graphene oxide composites. *Colloids Surf B.* 2013. **103**: 523.

39. Zhang Y., Liu Y., Wang X., Sun Z., Ma J., Wu T., Xing F., Gao J. Porous graphene oxide/carboxymethyl cellulose monoliths, with high metal ion adsorption. *Carbohydr. Polym.* 2014. **101**: 392.

40. Amphlett C.B. *Inorganic Ion Exchangers.* (Amsterdam: Elsevier, 1964).

41. Myronchuk V.G., Dzyazko Yu.S., Zmievskii Yu.G., Ukrainets A.I., Bildukevich A.V., Kornienko L.V., Rozhdestvenskaya L.M., Palchik A.V. Organic-inorganic membranes for filtration of corn distillery. *Acta Periodica Technologica.* 2016. **2016**(47): 153.

42. Zmievskii Yu., Rozhdestvenska L., Dzyazko Yu., Kornienko L., Myronchuk V., Bildukevich A., Ukrainetz A. Organic-inorganic materials for baromembrane separation. *Springer Proc. Phys.* 2017. **195**: 675.

43. Mal'tseva T.V., Kolomiets E.A., Vasilyuk S.L. Hybrid adsorbents based on hydrated oxides of Zr(IV), Ti(IV), Sn(IV), and Fe(III) for arsenic removal. *J. Water Chem. Technol.* 2017. **39**(4): 214.

44. Kolomiets E.A., Belyakov V.N., Palchik A.V. Maltseva T.V., Zheleznova L.I. Adsorption of arsenic by hybrid anion–exchanger based on titanium oxyhydrate. *J. Water Chem. Technol.* 2017. **39**(2): 80.

47. Maji S., Ghosh A., Gupta K., Ghosh A., Ghorai U., Santra A., Sasikumar P., Ghosh U.Ch. Efficiency evaluation of arsenic(III) adsorption of novel graphene oxide@iron-aluminium oxide composite for the contaminated water purification. *Sep. Purif. Technol.* 2018. **197**: 388.

48. Luo X., Wang Ch., Wang L., Deng F., Luo Sh., Tu X., Au Ch. Nanocomposites of graphene oxide-hydrated zirconium oxide for simultaneous removal of As(III) and As(V) from water. *Chem. Eng. J.* 2013. **220**: 98.

49. Wan Sh., He F., Wu J., Wan W., Gu Y., Gao B. Rapid and highly selective removal of lead from water using graphene oxide-hydrated manganese oxide nanocomposites. *J. Hazard. Mater.* 2016. **314**: 32.

50. Marcano D.C., Kosynkin D.V., Berlin J.M., Sinitskii A., Sun Z., Slesarev A., Alemany L.B., Lu W., Tour J.M. Improved synthesis of graphene oxide. *ACS Nano.* 2010. **4**(8): 4806.

51. Dzyazko Y.S., Volfkovich Y.M., Sosenkin V.E., Nikolskaya N.F., Gomza Yu.P. Composite inorganic membranes containing nanoparticles of hydrated zirconium dioxide for electrodialytic separation. *Nanoscale Res. Lett.* 2010. **9**(1): 271.

52. Meng F., Zhang X., Xu B., Yue Sh., Guo H., Luo Y. Alkali-treated graphene oxide as a solid base catalyst: synthesis and electrochemical capacitance of graphene/carbon composite aerogels. *J. Mater. Chem.* 2011. **21**: 18537.

53. Smettem K.R.J. Particle density. In: *Encyclopedia of soil science.* V. 2. (New York: Taylor and Francis Group, 2006).

54. Belyakov V.N., Rozhdestvenska L.M., Dzyazko Y.S. Electrodeionization of a Ni^{2+} solution using highly hydrated zirconium hydrophosphate. *Desalination.* 2006. **198**(1–3): 247.

55. Marhol M. Ion exchangers in analytical chemistry: their properties and use in inorganic chemistry. In: *Comprehensible analytical chemistry.* V. XIV. (Amsterdam: Elsevier, 1981).

56. Kang Ch., Wang Y., Li R., Du Y., Li J., Zhang B., Zhou L., Du Y. A modified spectrophotometric method for the determination of trace amounts of phenol in water. *Microchem. J.* 2000. **64** (2): 161.

57. Reeve R. *Introduction to Environmental Analysis.* (Chichester: Wiley, 2002).

58. Zhao J., Liu L., Li F. *Graphene Oxide: Physics and Applications.* (Heidelberg, New York, Dordrecht, London: Springer, 2015).

59. Kostrikin A.V., Spiridonov F.M., Komissarova L.N., Lin'ko I.V., Kosenkova O.V. On the structure and dehydration of hydrous zirconia and hafnia xerogels. *Russ. J. Inorg. Chem.* 2010. **55**(6): 866.

60. Kononenko N.A., Berezina N.P., Vol'fkovich Y.M., Shkol'nikov E.I., Blinov I.A. Investigation of ion-exchange materials structure by standard porosimetry method. *J. Appl. Chem. USSR.* 1985. **58**(10): 2029.

61. Volfkovich Yu.M., Sosenkin V.E., Nikolskaya N.F., Kulova T.L. Porous structure and hydrophilic-hydrophobic properties of gas diffusion layers of the electrodes in proton-exchange membrane fuel cells. *Russ. J. Electrochem.* 2008. **44**(3): 278.

62. Yang Z., Yan H., Yang H., Li H., Li A., Cheng R. Flocculation performance and mechanism of graphene oxide for removal of various contaminants from water. *Water Res.* 2013. **47**(9): 3037.

63. Rouquerol F., Rouquerol J., Sing H. *Adsorption by powders and porous solids. Principles, methodology and application.* (London, San Diego: Academic Press, 1999).

64. Goncharuk V.V., Dubrovina L.V., Kucheruk D.D., Samsoni-Todorov A.O., Ogenko V.M., Dubrovin I.V. Water purification of dyes by ceramic membranes modified by pyrocarbon of carbonized polyisocyanate. *J. Water Chem. Technol.* 2016. **38**(1): 34.

65. Goncharuk V.V., Dubrovina L.V., Kucheruk D.D., Samsoni-Todorov A.O., Ogenko V.M., Dubrovin I.V. Water purification of dyes by ceramic membrane modified by pyrocarbon from carbonized polymers. *J. Water Chem. Technol.* 2016. **38**(3): 163.